Improvement of the chemical content prediction of a model powder system by reducing multiple scattering using polarized light spectroscopy

R. Bendoula, Alexia Gobrecht, Bruno Moulin, Jean-Michel Roger, Véronique Bellon-Maurel

Author-produced version of the article published in Applied Spectroscopy, 2015, N°69(1), p.95-102
The original publication is available at http://www.ingentaconnect.com
http://dx.doi.org/10.1366/14-07539

Improvement of the chemical content prediction of a model powder system by reducing multiple scattering using polarized light spectroscopy

Ryad Bendoula,[1,*] Alexia Gobrecht,[1] Benoit Moulin,[1] Jean-Michel Roger [1] and Veronique Bellon-Maurel [1]

[1]Irstea, UMR ITAP, 361 rue J-F Breton, F-34196 Montpellier, France

[*]ryad.bendoula@irstea.fr

Abstract: Near Infrared Spectroscopy (NIRS) is a powerful non destructive analytical method used to analyze major compounds in bulk materials and products and requiring no sample preparation. It is widely used in routine analysis and also in-line in industries, in-vivo with biomedical applications or in-field for agricultural and environmental applications. However, highly scattering samples subvert Beer-Lambert law's linear relationship between spectral absorbances and the concentrations. Instead of spectral pre-processing, which is commonly used by NIR spectroscopists to mitigate the scattering effect, we put forward an optical method, i.e. coupling polarized light with NIR spectrometry, to free spectra from scattering effect. This should allow us to retrieve linear and steady conditions for spectral analysis. When tested in Visible-NIR (VIS-NIR) range (400-800 nm) on model media - mixtures of scattering and absorbing particles - the set-up provided

Author-produced version of the article published in Applied Spectroscopy, 2015, N°69(1), p.95-102
The original publication is available at http://www.ingentaconnect.com
http://dx.doi.org/10.1366/14-07539

significant improvements in absorber concentration estimation precision as well as in the quality and robustness of the calibration model.

Index Heading: Polarized Light Spectroscopy, Multiple Light Scattering, Diffuse Reflectance, Optical Properties, Chemical Content Prediction.

1. Introduction

Visible - Near infrared spectroscopy (VIS-NIRS) is a well-known technique used for measuring the chemical composition of a wide variety of media and products. Although VIS-NIRS has been quoted in articles for approximately 50 years[1,2] with this purpose, it really took off in the late 80's in agricultural and food applications (jumping from around 10 publications per year in the late 80's to 150 publications per year in the turn of century), and then in the 90's for pharmaceutical and biomedical applications. Today, it plays a major role in these sectors, as a routine laboratory method for in vivo or in-line monitoring system. On the one hand VIS-NIRS presents several advantages: VIS-NIR extinction coefficients are small compared to mid-infrared (MIR) ones, which allows light to penetrate deeper into objects and avoids time-consuming sample preparation; VIS-NIR light scattering makes it possible to analyze bulk samples with a retro-diffusion optical configuration, thus turning it into a non-destructive technique. In addition VIS-NIR optical components are low cost and with high Signal-to-Noise Ratio (SNR). On the other hand, VIS-NIRS has several drawbacks: the VIS-NIR spectrum is poorly resolved as it is made up of scattering effects and of wide low-intensity harmonics and combinations of MIR

Author-produced version of the article published in Applied Spectroscopy, 2015, N°69(1), p.95-102
The original publication is available at http://www.ingentaconnect.com
http://dx.doi.org/10.1366/14-07539

fundamental absorption bands. Consequently, retrieving chemical information from VIS-NIR spectra is quite painstaking and requires advanced chemometrics: it is based on calibration models to be built between VIS-NIR spectra and known concentrations of a set of calibration samples. Traditionally, linear multivariate calibration methods such as Principal Component Regression (PCR) and Partial Least Square Regression (PLSR) are used in VIS-NIRS. However, scattering effects are troublesome in the VIS-NIR spectra of turbid media, defined by Shi and Anderson[3] as "*samples exhibiting multiple scattering events*". Scattering can be several orders of magnitude larger than absorption[4] and may invalidate the use of such data processing methods, which are themselves based on the underlying assumption of a linear Beer-Lambert law relationship between absorbance spectra and chemical concentration[5]. It is therefore necessary for VIS-NIR spectroscopists working on highly scattering media to use strategies to release VIS-NIR spectra from scattering effects. The most common strategy is spectral pre-treatment. These preprocessing step is specifically designed to reduce multiplicative and additive effects caused by variations in sample physical properties[6,7] . Among them, standard normal variate (SNV) often associated to detrend[8], multiplicative signal correction (MSC)[9], Extended MSC (EMSC)[7], normalization or Optical Path Length Estimation and Correction (OPLEC)[5,10]. However, these approaches remain questionable: they consider that scattering is nearly constant over the wavelengths, which is not the case[3]; they may eliminate chemical-related information, which is very small with

Author-produced version of the article published in Applied Spectroscopy, 2015, N°69(1), p.95-102
The original publication is available at http://www.ingentaconnect.com
http://dx.doi.org/10.1366/14-07539

regard to scattering effects[11]; they are inappropriate when light scattering varies greatly from sample to sample[12].

Another option is to acquire the spectrum in a way that separates the part related to absorption from the part related to scattering. Specific experimental techniques, related to the application of light propagation theory and resolution of the Radiative Transfer Equation[3] have been proposed, including adding-doubling set-ups[12-14], spatially-resolved spectroscopy[15], time-resolved spectroscopy[4,16] and frequency-resolved spectroscopy[17].

Although powerful, these methods have their limitations, particularly when applied on highly turbid samples. First, they may require complex and sometimes expensive optical implementations, which may not be compatible with conventional spectrometers or with highly turbid samples (for which transmission measurement is not possible). Secondly, as they rely on the estimation of absorption and scattering coefficients achieved by model inversion, parameters describing the studied medium (sample thickness, refractive index, particle size and shape...) must be known or approximated, which may be a troublesome task as they are often unknown in complex media[12,18].

Whereas separating absorption and scattering from a VIS-NIR signal is still an open research issue on highly turbid samples, the main demand from VIS-NIR spectroscopists is *merely* for spectra with reduced impact of scattering in order to better fit Beer-Lambert's Law conditions[19,20].

Author-produced version of the article published in Applied Spectroscopy, 2015, N°69(1), p.95-102
The original publication is available at http://www.ingentaconnect.com
http://dx.doi.org/10.1366/14-07539

Light polarization subtraction is a simple technique to reduce directly the effects of multi-scattering on the measured signal[20,21]. This approach has been based on the fact that, when light interacts with matter, a small number of scattering events do not significantly modify the polarization status of the beam whereas multiple scattering leads to depolarization[18,22]. Polarization subtraction technique[19,23-25] was used to select light beams that retain initial polarization and which are therefore less impacted by multiple scattering events.

Although this technique has gained interest in the field of biomedical [20,21,25], where it is used to optically target subsurface organelles (particles suspended in water) and tissues (layered samples), it is either poorly understood or not used by NIR spectroscopists working with agricultural, food, pharmaceutical and other industrial samples. To our knowledge, polarized NIRS techniques have never been applied to routine or in-line analysis to reduce scattering effects on spectra on turbid media.

In this paper, the effectiveness of this multi-scattering correction based on the polarization subtraction is evaluated using a two-component model powder system. The objectives of this paper were to assess the effect of multi-scattering correction (i) on the performances of a calibration model and (ii) on the robustness of the prediction model built from the corrected spectra for predicting the absorber's concentration of powder samples

2. Theoretical Model : Polarization subtraction

Author-produced version of the article published in Applied Spectroscopy, 2015, N°69(1), p.95-102
The original publication is available at http://www.ingentaconnect.com
http://dx.doi.org/10.1366/14-07539

Capital bold characters will be used for matrices, e.g. **X**; non bold characters will be used for column vectors, e.g. X

Polarization subtraction technique[23-25] is based on the polarization-maintaining property of weakly scattered light. When polarized light illuminates a scattering medium, weakly scattered light will emerge in its original polarization state[21,26-28], while multiple scattered light will emerge with random polarization. In the case of linearly polarized source, the light that is remitted in the same polarization channel as the input illumination is composed by light that has maintained its original polarization state plus a component from the randomly polarized heavily scattered light (cf equation 1). Light that emerges in the orthogonal polarization channel contains only randomly polarized light, approximately equal to the randomly polarized component in the original polarization state (cf equation 2).

$$I_{\parallel}(\lambda) = \frac{\Omega}{2\pi}.I_0(\lambda).S(\lambda) + \frac{\Omega}{2\pi}.I_0(\lambda).\alpha(\lambda).M(\lambda) \quad (1)$$

$$I_{\perp}(\lambda) = \frac{\Omega}{2\pi}.I_0(\lambda).\beta(\lambda).M(\lambda) \quad (2)$$

Where $I_{\parallel}(\lambda)$ and $I_{\perp}(\lambda)$ are the light scattered by the media with parallel and perpendicular polarization respect to the polarization of the illumination light. $I_0(\lambda)$ is the intensity of the illumination light. Ω is the collection solid angle, residual term of the integration on the solid angle[23-25], of the optical device. $S(\lambda)$ and $M(\lambda)$ are the probabilities of light undergoing single and multiple scattering respectively.

Since all light undergoes scattering :

Author-produced version of the article published in Applied Spectroscopy, 2015, N°69(1), p.95-102
The original publication is available at http://www.ingentaconnect.com
http://dx.doi.org/10.1366/14-07539

$$S(\lambda) + M(\lambda) = 1 \quad (3)$$

Finally, $\alpha(\lambda)$ and $\beta(\lambda)$ are the multiple light scattered ratio by the media with the parallel and perpendicular polarization respect to the polarization of the illumination light. The sum $\alpha(\lambda)$ and $\beta(\lambda)$ must be one:

$$\alpha(\lambda) + \beta(\lambda) = 1 \quad (4)$$

By subtracting (1) to (2), the intensity of light undergoing single scattering ($I_{ss}(\lambda)$) is equal to :

$$I_{ss}(\lambda) = I_{\parallel}(\lambda) - I_{\perp}(\lambda) = \frac{\Omega}{2\pi}.I_0(\lambda).[S(\lambda) + (\alpha(\lambda) - \beta(\lambda)).M(\lambda)] \quad (5)$$

In conclusion, the part of the single-scattering effect in the signal is preserved and the multi-scattering effect is highly reduced.

3. Materials and Methods

3.1 Instrumentation

In the experimental setup (figure 1), a halogen light source (150 W, Leica Cls) was coupled with a 940 µm core diameter optical fiber (numerical aperture (N.A) 0.22, Sedi & ATI). The light delivered by the fiber was collimated by an aspheric lens (F220SMA-B - Thorlabs). The incident beam was a 2 cm diameter circular spot with 1° divergence. The incident and reflected beam were polarized thought two broad-band (400 nm - 800nm) polarizers (NT52-557, Edmunds Optics). Incident light was

Author-produced version of the article published in Applied Spectroscopy, 2015, N°69(1), p.95-102
The original publication is available at http://www.ingentaconnect.com
http://dx.doi.org/10.1366/14-07539

linearly polarized and reflected light was collected in a narrow cone (1°). The output from the analyzer was coupled inside an optical fiber (N.A 0.22, Sedi & ATI) by an aspheric lens (F220SMA-B - Thorlabs). This fiber was connected to a spectrometer (MMS1, Zeiss) featuring a detection range of 400 nm - 800 nm, with 3 nm resolution. A constant angle of 70° was maintained between the excitation and collection arms. This angle was chosen to optimize intensity of the reflected beam and to avoid specular reflection.

3.2 Experimental design and sample preparation

Powdered samples mixing sand (Fontainebleau sand VWR International) and coloring dyes (brilliant blue FCF-E133 and chlorophyllin E141, purchased from Colorey, respectively named E133 and E141 in the text) were prepared. Two sand particle size classes were used: S_1 with a diameter less than 250 µm and S_2 with a diameter greater than 250 µm. Sand play the role of a scattering but non absorbing matrix. One or both of the coloring dyes have been added at different densities to the sand, playing the role of absorbing substance in the mixture. Note that absorbers in powdered form also have scattering properties. Particle sizes of the coloring powders were less than 50µm, with E133 being about three times smaller than E141.

Overall, 42 samples were prepared for spectral acquisition composing a calibration set and 12 samples were prepared, afterward and with the same procedure to create an independent test set.

The range of sample's colorant densities (in g.L-1) is specified in figure 2.

Author-produced version of the article published in Applied Spectroscopy, 2015, N°69(1), p.95-102
The original publication is available at http://www.ingentaconnect.com
http://dx.doi.org/10.1366/14-07539

Each sample was directly prepared in an airtight plastic container of 100 mL by adding the precisely weighted corresponding amount of colorant in 20 g of sand using an analytical balance (Kern 770). The maximum dye volume added was not higher than 4% of the total sand volume. Considering that the pore volume for sand is about 40%, and that the dye particles are between 5 to 10 times smaller than the sand, one can make the assumption that the dye would fill the interstices between the sand particles and therefore not increase the initial volume of sand. The density of the colorant d_{dye} in a sample was obtained from :

$$d_{dye} = \frac{m_{dye}.d_{sand}}{m_{sand}} \quad (6)$$

With m_{dye} the added mass of dye, d_{sand} the density of sand (which differ for S_1 and S_2) and m_{sand} the mass of sand (here 20 g). The colorant density ranged from [0 - 18 $g.L^{-1}$].

To ensure homogeneity of the mixture, the sample was agitated after preparation and again just before it was carefully transferred in an adapted 5 cm of diameter cup to get an even and horizontal surface.

3.3 Spectral acquisition

For each sample, light was measured with the polarized spectrometer with parallel and perpendicular respect to the polarization of the illumination light. Dark current (I_b) was recorded from all measured spectra and subtracted.

A broadband dielectric mirror (BB3-E02, Thorlabs) was used as a reference (I_0) to standardize spectra from non-uniformities of all components of the instrumentation (light source, fibers, lens, polarizer and spectrometer).

Author-produced version of the article published in Applied Spectroscopy, 2015, N°69(1), p.95-102
The original publication is available at http://www.ingentaconnect.com
http://dx.doi.org/10.1366/14-07539

From these measurements and the equation (5), a raw reflectance (R_w) and a corrected reflectance (R_c), for each sample, were calculated :

$$R_w(\lambda) = \frac{(I_{\parallel}(\lambda) - I_{b\parallel}(\lambda)) + (I_{\perp}(\lambda) - I_{b\perp}(\lambda))}{(I_{0\parallel}(\lambda) - I_{b\parallel}(\lambda))} \quad (7)$$

$$R_c(\lambda) = \frac{(I_{\parallel}(\lambda) - I_{b\parallel}(\lambda)) - (I_{\perp}(\lambda) - I_{b\perp}(\lambda))}{(I_{0\parallel}(\lambda) - I_{b\parallel}(\lambda))} = \frac{I_{ss}(\lambda) - (I_{b\parallel}(\lambda) + I_{b\perp}(\lambda))}{(I_{0\parallel}(\lambda) - I_{b\parallel}(\lambda))} \quad (8)$$

With $I_{\parallel}(\lambda)$ and $I_{\perp}(\lambda)$ the intensities of light scatters by the media with parallel and perpendicular polarization respect to the polarization of the illumination light and $I_{0\parallel}(\lambda)$ and $I_{0\perp}(\lambda)$, the intensities of light reflected by the standard mirror with parallel polarization respect to the polarization of the illumination light (as the perpendicular component emerging from the mirror is zero). $I_{b\parallel}(\lambda)$and $I_{b\perp}(\lambda)$ are the dark current intensities recorded for each measurement.

3.4 Multivariate analysis

All computations and multivariate data analysis were performed with Matlab software v. R2012b (The Mathworks Inc., Natick, MA,USA).

3.5 Linear unmixing

The first step of Classical Least Square (CLS)[29] was used to extract the reflectance *pure spectra* of the absorbers from the reflectance spectra of the mixtures. Also called **K**-matrix, this linear unmixing assumes that a spectrum is a linear combination of the pure component's spectra. The whole calibration set **R** (42 samples mixing the

Author-produced version of the article published in Applied Spectroscopy, 2015, N°69(1), p.95-102
The original publication is available at http://www.ingentaconnect.com
http://dx.doi.org/10.1366/14-07539

absorbers at different concentrations) and **C**, the matrix of sample components concentrations, were used to compute the linear least square estimated $\widehat{\mathbf{K}}$-matrix of the two pure active components (E133 and E141) composing **K** knowing that:

$$\widehat{\boldsymbol{K}} = \boldsymbol{R}\boldsymbol{C}^{\boldsymbol{T}}(\boldsymbol{C}\boldsymbol{C}^{\boldsymbol{T}})^{-\mathbf{1}} \quad (9)$$

Both the raw reflectance spectra ($\mathbf{R_w}$) and the corrected reflectance spectra ($\mathbf{R_c}$) were used to compute respectively $\widehat{\mathbf{K_w}}$ and $\widehat{\mathbf{K_c}}$ containing the demixed pure spectra of E133 and E141.

3.6 Calibration

Partial Least Square (PLS)[30] algorithm was used to model the chemical composition of the powder mixture using $\mathbf{R_w}$ and $\mathbf{R_c}$. A general PLS model was built using the whole calibration set (42 samples) to predict the samples of the independent test set (12 samples). Secondly, to assess the robustness of the prediction models regarding sand particle size, a PLS model was built with the samples set S_2 and tested on the independent test set S_1 (figure 2). The number of latent variables was determined by comparing performances by leave-one-out cross-validation[31]. Performances (R^2, Standard Error of prediction corrected from the biais (SEPc)) and number of latent variables of the different prediction models built with uncorrected and corrected signals were compared when applied on the test set.

4. Results and discussion

Author-produced version of the article published in Applied Spectroscopy, 2015, N°69(1), p.95-102
The original publication is available at http://www.ingentaconnect.com
http://dx.doi.org/10.1366/14-07539

4.1 Spectra analysis

Bulk colorant

The raw spectra $R_w(\lambda)$ and the corrected spectra $R_c(\lambda)$ of the pure powder colorant E133 and E141 are represented in figure 3 (a) and (b).

First comment is that the polarization subtraction reduces the global reflectance intensity of the measured signal (by 10 times). It is an expected result as only a small part of the signal is selected: the single-scattered one. Despite this reflectance loss, the corrected spectrum is not noisy and contains information about the sample.

Between 400 nm and 700 nm, the raw spectrum and the corrected spectrum have similar shapes. For example, the spectroscopic signature of the colorant E133 appears to be purple (as seen in powdered form), mixing a reflectance peak at 450 nm (Blue) and at 650 nm (Red). However, these peaks are more marked in the corrected spectra. For the raw spectrum, crushing peaks can be explained by a strong increase in reflectance after 750 nm. This sharp increase in reflectance, in a spectral range where the colorant does not absorb, is due to the multi-scattering. However, this effect seems to be less important for E141 than for E133. In the corrected spectra, this effect is strongly reduced (figure 3 (b)).

Sand and dye mixtures

Figures 3 (c) and (d) show respectively the raw spectra and the corrected spectra of sand S_1 mixing coloring powder E133 at different densities. When mixed with the colorant, sand is responsible for high multi-scattering as it is not absorbing the light.

Author-produced version of the article published in Applied Spectroscopy, 2015, N°69(1), p.95-102
The original publication is available at http://www.ingentaconnect.com
http://dx.doi.org/10.1366/14-07539

This physical phenomenon comes on top of the chemical information contained in the spectra and masks the spectral features of the absorber. The shape of the raw spectra of coloring powder E133 (figure 3 (a)) and the shapes of the raw reflectance of the sand-dye mixture (figure 3 (c)) are completely different. The multiplicative effect due to scattering is not wavelength dependent and depends on the number of scatterers in the sample. Therefore, the more dye, the more scatterers and, consequently the higher the reflectance. The order of the raw spectra is consistent with the dye's concentration, but for a physical reason.

By applying the correction, the spectral features of the colorant are enhanced as it can be seen on figure 3 (d). The signature of the corrected spectra is similar to the spectral signal of the colorant E133 in powdered form (figure 3 (b)). The reflectance peaks at 450 nm and at 650 nm clearly appear, but more important, because linked to the dye's concentration, the wavelength regions where absorbance occurs (400- 430 nm and 500 – 650 nm) are now visible. In these regions, the spectrum ordering is consistent with the dye concentration, contrary to the other areas where low absorbance occurs and reveals more complex reflectance patterns.

Figures 3 (e) and (f) show respectively the raw spectra and the corrected spectra of sand S_1 mixing this time coloring powder E141 at different densities. By comparing the raw reflectance intensities of the sand - E133 mixtures (figure 3 (c)) and sand - E141 mixtures (figure 3 (e)), containing the same ranges of dye's densities, it appears that the level of R_w is two-times higher for E133 than for E141. As stated in section 'Experimental design and sample preparation', the particle size of E141 is, at least,

Author-produced version of the article published in Applied Spectroscopy, 2015, N°69(1), p.95-102
The original publication is available at http://www.ingentaconnect.com
http://dx.doi.org/10.1366/14-07539

three-times larger than E133. This difference in particle diameter has a direct impact on the elastic scattering phenomenon occurring during light-matter interaction. First, for the same density of dye, small particles scatter more than larger particles[21]. Secondly, the scattering angle differs between small and large particles: the larger the diameter, the smaller the scattering angle. Combining these two properties, the overall reflectance intensity will be higher for smaller particles, which is the case of raw reflectance of the Sand-E133 mixture.

For the corrected spectra R_c, there is no significant difference in the intensity level between sand - E133 mixtures (figure 3 (d)) and sand - E141 mixtures (figure 3 (f)). This is coherent with the fact that the method corrects the spectra from multi-scattering, which is mainly due to the sand particles but also, and in a significant manner, to the powdered colorant.

4.2 Extraction of the absorber's pure spectra

Figure (4) presents the demixed pure spectra $\widehat{\boldsymbol{K}}$ extracted from the reflectance spectra ($\mathbf{R_w}$ and $\mathbf{R_c}$). The linear unmixing (figure 4 (a)) applied to raw spectra ($\mathbf{R_w}$) provided estimated pure spectra ($\widehat{K_{w\_E133}}(\lambda)$ and $\widehat{K_{w\_E141}}(\lambda)$) that a very different from the raw spectra $R_{w\_E133}(\lambda)$ and $R_{w\_E141}(\lambda)$ measured directly on the powders. The shape of these spectra are not matching and the correlation coefficients, between $\widehat{K_{w\_E133}}(\lambda)$ and $R_{w\_E133}(\lambda)$ and between $\widehat{K_{w\_E141}}(\lambda)$ and $R_{w\_E141}(\lambda)$, are respectively equal to 0.59 and 0.74.

Author-produced version of the article published in Applied Spectroscopy, 2015, N°69(1), p.95-102
The original publication is available at http://www.ingentaconnect.com
http://dx.doi.org/10.1366/14-07539

Linear unmixing assumes that a spectrum is a linear combination of the pure components spectra. From these results, the failure to recover the absorber's pure spectrum from the raw reflectance spectra, support the fact that interactions in the mixture are responsible of non-linearities which are directly responsible of the non-linearities in the relationship between the absorbance and the absorbing power of the sample. It is well known[20,32] that scattering and absorbance are not independent phenomenon. Scatter increases the mean free path of photons, which increases the chances of being absorbed.

On the contrary, the computation of the $\widehat{\mathbf{K_c}}$-matrix is successful and matches the pure colorant corrected reflectance spectrum. Estimated pure spectra ($\widehat{K_{c\_E133}}(\lambda)$ and $\widehat{K_{c\_E141}}(\lambda)$) are very close to $R_{c\_E133}(\lambda)$ and $R_{c\_E141}(\lambda)$ measured directly on the powder and corrected. The correlation coefficients are respectively 0.98 and 0.93. As the method corrects the signal from a physical phenomenon (multi-scattering), one can affirm that the observed interactions in the raw spectra are of optical nature (and not chemical interactions). Regarding these results and this consideration, polarization subtraction correction induces, by reducing the multi-scattering effect, a better linear relationship between the light attenuation and the absorption the dyes. The recovered spectra $\widehat{K_c}$ are corrected from the physical interactions occurring in the mixture.

4.3 Calibration model

General model

Author-produced version of the article published in Applied Spectroscopy, 2015, N°69(1), p.95-102
The original publication is available at http://www.ingentaconnect.com
http://dx.doi.org/10.1366/14-07539

Table 1 shows the quality parameter of the prediction models of the test set absorber's densities comparing the raw and the corrected spectra.

First, with the raw spectra $R_w(\lambda)$, the quality of the E133 prediction model is distinctly poorer than the quality of the E141 prediction model. The number of latent variables is much higher for E133 as well as the SEP_c. On the contrary, the figures of merit for the E141 model are good. Again, E133 and E141 behave differently. As stated before, multiscattering effect is more important when E133 is present in the mixture (with or without E141) because of a smaller particle diameter. Hence, non-linearities between absorbance and absorber's concentration are more important and the PLS model is limited in building a performant linear prediction model for E133.

When the models are built with the corrected reflectance spectra $R_c(\lambda)$, the figure of merit of the absorber's density prediction models are good and of the same level for E133 and E141. In both cases, the number of latent variables is decreasing. The improvement is less important for E141 but significant for E133. And both models have a lower standard error of prediction compared to the $R_w(\lambda)$ prediction models for the two colorants. In section ‘Sand and dye mixture’, we stated that the proposed method mainly reduced the effect of multiscattering due to sand particles, enhancing the part of the signal related to chemical absorbance. In $R_w(\lambda)$, while this information is present, it is masked by the multi-scattering and the PLS needs more latent variable to extract this chemically related information to build a model.

Here, the different behavior of the two dyes is not obvious anymore. This agrees with the hypothesis that the correction method equalizes the mean free photon path

Author-produced version of the article published in Applied Spectroscopy, 2015, N°69(1), p.95-102
The original publication is available at http://www.ingentaconnect.com
http://dx.doi.org/10.1366/14-07539

between all the samples, regardless of the particle size and shape of the sample's constituents. For the two absorbers, the number of latent variables, which is an indicator of the complexity of the models, is still high (respectively 5 and 4 for E133 et E141 with the corrected spectra $R_c(\lambda)$) for samples mixing only two different absorbers. Theoretically, two PLS components should be sufficient. This agrees with the initial assumption that the polarization subtraction method highly reduces the multi-scattering but does not remove it completely. In addition, these results are consistent with the conclusions of section 'Extraction of the absorber's pure spectra', stating that the correction method restores, in a significant manner, the linear relationship between the spectra and the absorber's density in the powdered samples.

To conclude, as the PLS models using the corrected spectra show good prediction capacities, it fulfills the assumption that even if the corrected signal intensity is highly reduced, the remaining information is of better quality in terms of signal sensitivity.

Robustness assessment

Table 2 presents the results of the calibration model built with samples of one particle size ($S_2 > 250$ µm) and tested on samples with another particle size ($S_1 < 250$ µm).

First, the models built with $R_w(\lambda)$ show, as previously observed, better predictions for E141 than for E133, but, in overall, lower quality than in table 1. This confirms a different behavior of E133 and E141, but also that the sand particle size has an effect

Author-produced version of the article published in Applied Spectroscopy, 2015, N°69(1), p.95-102
The original publication is available at http://www.ingentaconnect.com
http://dx.doi.org/10.1366/14-07539

in the quality of the predictions. A change in the physical structure of the samples usually leads to low prediction performances because of the scattering impact on the signal.

When built with the corrected spectra, again, the prediction of E133 highly improves, while the gain is less significant for E141, which is also consistent with the previous conclusions. But overall, the predictions are good, confirming that the corrected spectra, composed by the single scattered part of the total reflectance signal, becomes less dependent to physical changes in the sample.

The polarization subtraction method selects by optical means only, part of information related to the powdered absorbers concentration, while discarding the unwanted effect of multi-scattering on the signal. The measured signal becomes less dependent of the particle size changes of the samples and therefore improves both quality and robustness of the prediction models.

5. Conclusion

This study demonstrates the effectiveness of the polarized light subtraction method, applied to a two component model powder system, which improves the performance of multivariate calibration models.

By selecting only the light which has conserved the initial polarization and therefore being less impacted by scattering events, the collected photons all have the same mean free pathlength. As a consequence, the linear relationship between the spectra and the absorbers concentration is restored.

Author-produced version of the article published in Applied Spectroscopy, 2015, N°69(1), p.95-102
The original publication is available at http://www.ingentaconnect.com
http://dx.doi.org/10.1366/14-07539

Then it is possible, by using Linear Unmixing to recover the pure spectra of the dyes. These recovered spectra are corrected from the physical interactions occurring in the mixture.

When the corrected spectra are used to build the PLS models, all the general quality parameters and the parsimony improve, especially for highly scattering media. Although the overall signal intensity is reduced after optical correction, the remaining information in the corrected signal is sufficient and of better quality to build a good prediction model, thus meaning that the signal sensitivity increases. Inevitably there is a trade-off between making more accurate measurements and a reduction of SNR.

After the polarization correction, the measured signal becomes less dependent to physical changes (particle sizes) which also improve the robustness of the prediction models.

This "plug and play" optical method offers the potential to be easy to implement to a commercial spectrophotometry system and does not significantly increase the measurement time.

References and links

(1) Hart, J.; Norris, K.; Golumbic, C. Cereal Chem 1962, 39, 94–99.

(2) Massie, D. R.; Norris, K. H. Transactions of the ASABE 1965, 8 (4), 598–600.

(3) Shi, Z.; Anderson, C. A. Journal of Pharmaceutical Sciences 2010, 99, 4766–4783.

(4) Chauchard, F.; Roger, J.; Bellon-Maurel, V.; Abrahamsson, C.; Andersson-Engels, S.; Svanberg, S. Applied Spectroscopy 2005, 59, 1229–1235.

(5) Jin, J.-W.; Chen, Z.-P.; Li, L.-M.; Steponavicius, R.; Thennadil, S. N.; Yang, J.; Yu, R.-Q. Analytical Chemistry 2012, 84, 320–326.

(6) Rinnan, A.; Berg, F. v. d.; Engelsen, S. B. TrAC Trends in Analytical Chemistry 2009, 28, 1201–1222.

(7) Martens, H.; Stark, E. Journal of Pharmaceutical and Biomedical Analysis 1991, 9, 625–635.

(8) Barnes, R. J.; Dhanoa, M. S.; Lister, S. J. Appl. Spectrosc. 1989, 43, 772–777.

(9) Geladi, P.; MacDougall, D.; Martens, H. Appl. Spectrosc. 1985, 39, 491–500.

(10) Chen, Z.-P.; Morris, J.; Martin, E. Analytical Chemistry 2006, 78, 7674–7681.

(11) Martens, H.; Nielsen, J. P.; Engelsen, S. B. Analytical Chemistry 2003, 75, 394–404.

(12) Steponavicius, R.; Thennadil, S. N. Analytical Chemistry 2011, 83, 1931–1937.

(13) Prahl, S. Optical-thermal response of laser-irradiated tissue, A 1995, 122–127.

(14) Steponavicius, R.; Thennadil, S. N. Analytical Chemistry 2009, 81, 7713–7723.

(15) Farrell, T.; Patterson, M.; Wilson, B. Medical Physics 1992, 19, 879–888.

(16) Abrahamsson, C.; Johansson, J.; Andersson-Engels, S.; Svanberg, S.; Folestad, S. Analytical Chemistry 2005, 77, 1055–1059.

(17) Torrance, S.; Sun, Z.; Sevick-Muraca, E. Journal of Pharmaceutical Sciences 2004, 93,1879–1889.

(18) Swartling, J.; Dam, J.; Andersson-Engels, S. Applied Optics 2003, 42, 4612–4620.

(19) Hebden, J. C.; Arridge, S. R.; Delpy, D. T. Physics in Medicine and Biology 1997, 42, 825.

(20) Lu, B.; Morgan, S. P.; Crowe, J. A.; Stockford, I. M. Appl. Spectrosc. 2006, 60, 1157–1166.

(21) Backman, V.; Gurjar, R.; Badizadegan, K.; Itzkan, I.; Dasari, R. R.; Perelman, L. T.; Feld, M. Selected Topics in Quantum Electronics, IEEE Journal of 1999, 5, 1019–1026.

(22) Abrahamsson, C.; Löwgren, A.; Strömdahl, B.; Svensson, T.; Andersson-Engels, S.; Johansson, J.; Folestad, S. Appl. Spectrosc. 2005, 59, 1381–1387.

(23) Schmitt, J.; Gandjbakhche, A.; Bonner, R. Appl. Opt. 1992, 31, 6535–6546.

(24) Morgan, S.; Ridgway, M. Optics Express 2000, 7, 395–402.

(25) Demos, S. G.; Alfano, R. R. Appl. Opt. 1997, 36, 150–155.

(26) Demos, S. G.; Alfano, R. R. Opt. Lett. 1996, 21, 161–163.

(27) Sokolov, K.; Drezek, R.; Gossage, K.; Richards-Kortum, R. Opt. Express 1999, 5, 302–317.

(28) Yoo, K.; Alfano, R. Physics Letters A 1989, 142, 531–536.

(29) Geladi, P. Spectrochimica Acta Part B: Atomic Spectroscopy 2003, 58, 767 – 782.

(30) Wold, S.; Sjöström, M.; Eriksson, L. Chemometrics and Intelligent Laboratory Systems 2001, 58, 109–130.

452 (31) Wold, S. Technometrics 1978, 20, 397–405.

453 (32) Stockford, I. M.; Lu, B.; Crowe, J. A.; Morgan, S. P.; Morris, D. E. Appl.

454 Spectroscopy 2007, 61, 1379–1389.

455

Author-produced version of the article published in Applied Spectroscopy, 2015, N°69(1), p.95-102
The original publication is available at http://www.ingentaconnect.com
http://dx.doi.org/10.1366/14-07539

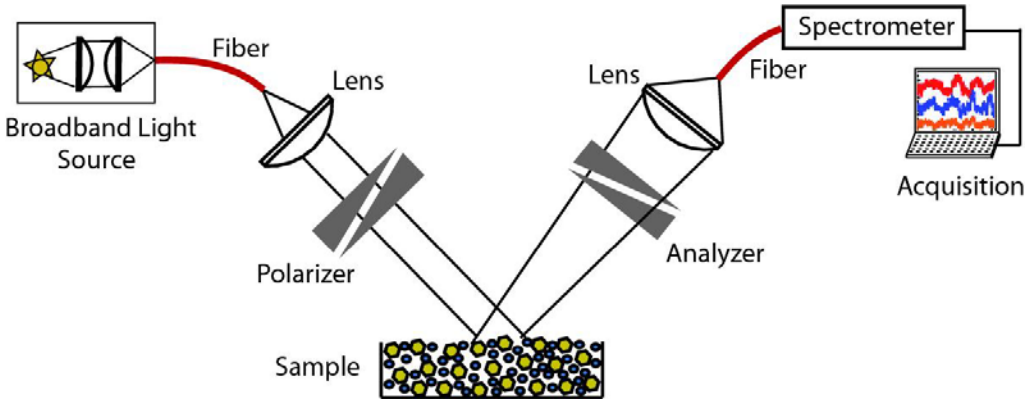

Figure 1: Schematic diagram of polarized light spectroscopy system.

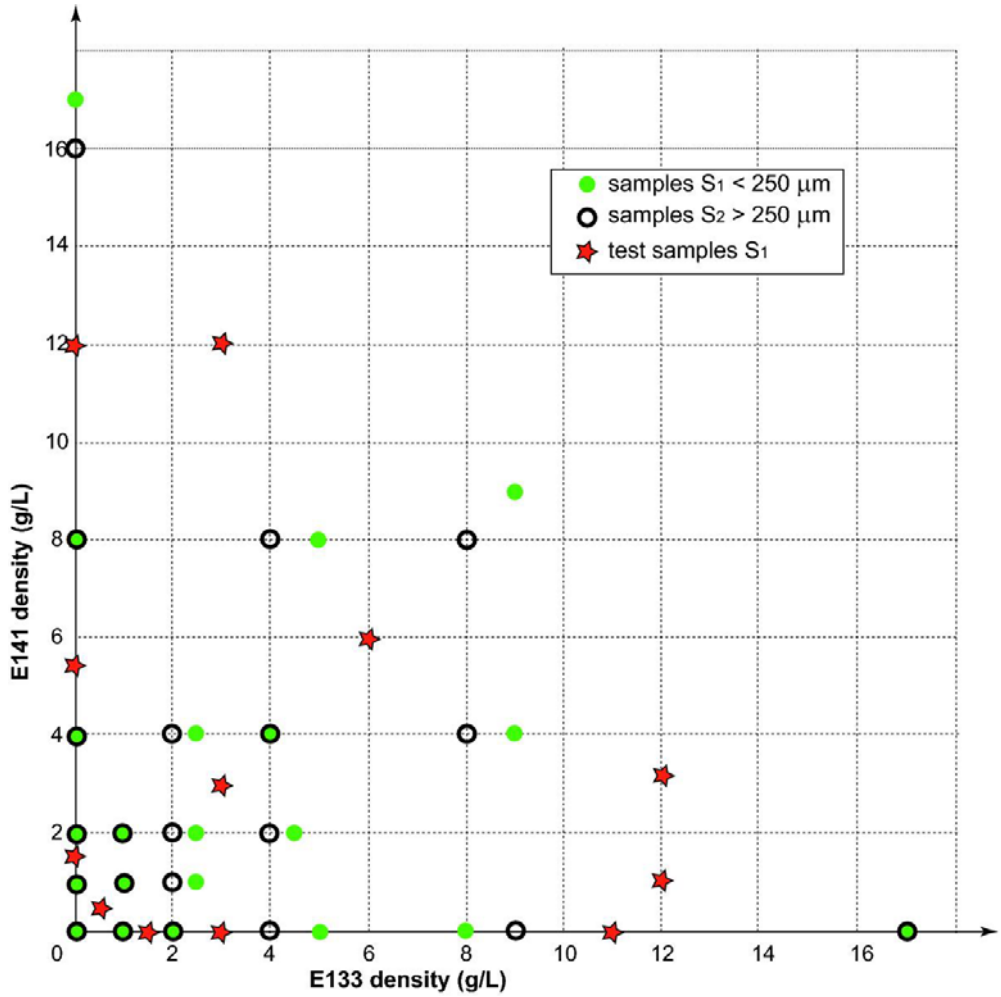

Figure 2: Experimental design presenting the dye densities in $g.L^{-1}$ of 42 samples for the calibration set and 12 samples for the independent test set.

Author-produced version of the article published in Applied Spectroscopy, 2015, N°69(1), p.95-102
The original publication is available at http://www.ingentaconnect.com
http://dx.doi.org/10.1366/14-07539

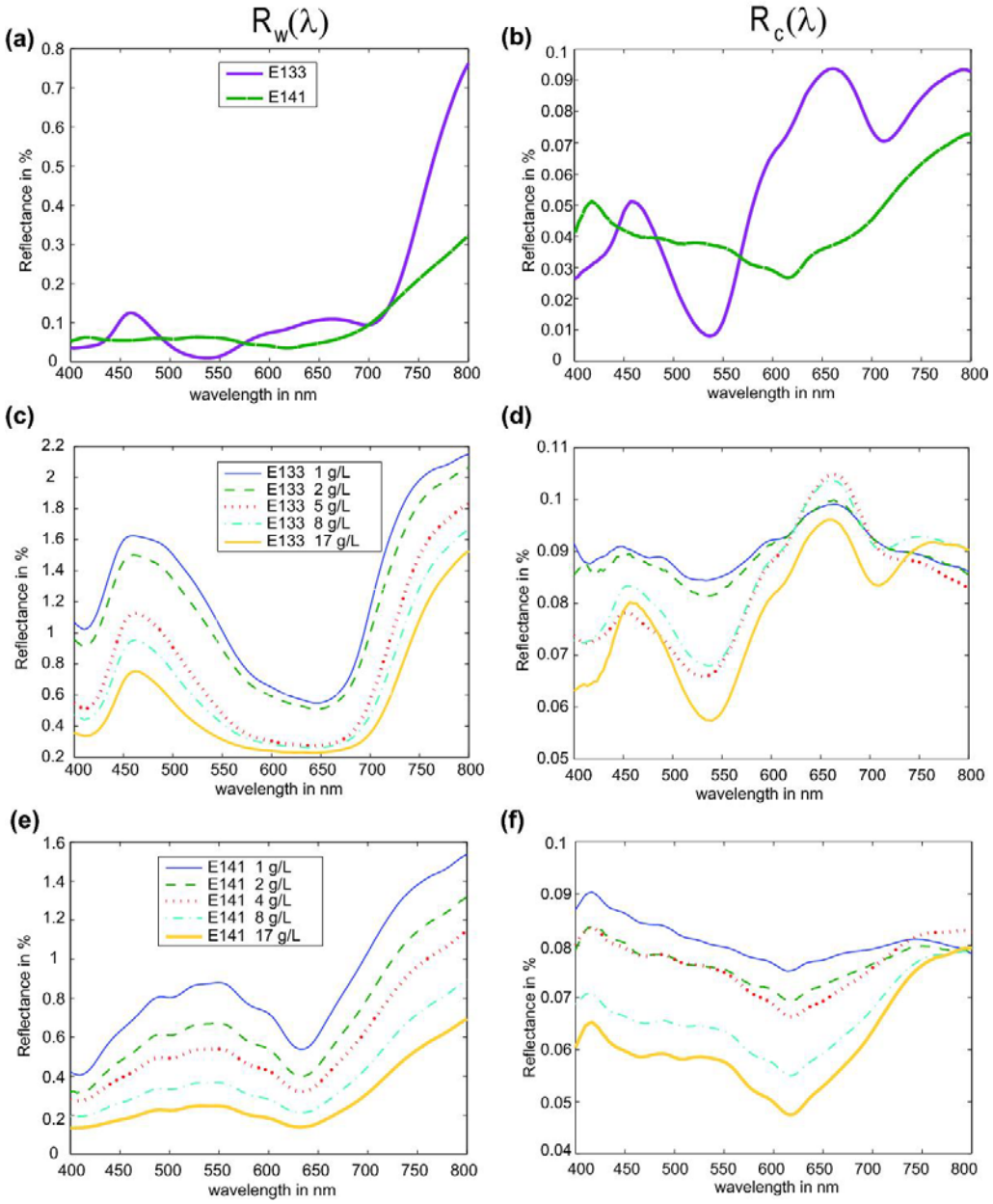

Figure 3: (a) Raw reflectance spectra of coloring powder E133 and E141. (b) Corrected reflectance spectra of coloring powder E133 and E141 (c) Raw reflectance spectra of sand S_1 + coloring powder E133 mixed at different densities. (d) Corrected reflectance spectra of sand S_1 + coloring powders E133 mixed at different densities.(e) Raw reflectance spectra of sand S_1 + coloring powder E141 mixed at different densities.(f) Corrected reflectance spectra of sand S_1 + coloring powders E141 mixed at different densities.

Author-produced version of the article published in Applied Spectroscopy, 2015, N°69(1), p.95-102
The original publication is available at http://www.ingentaconnect.com
http://dx.doi.org/10.1366/14-07539

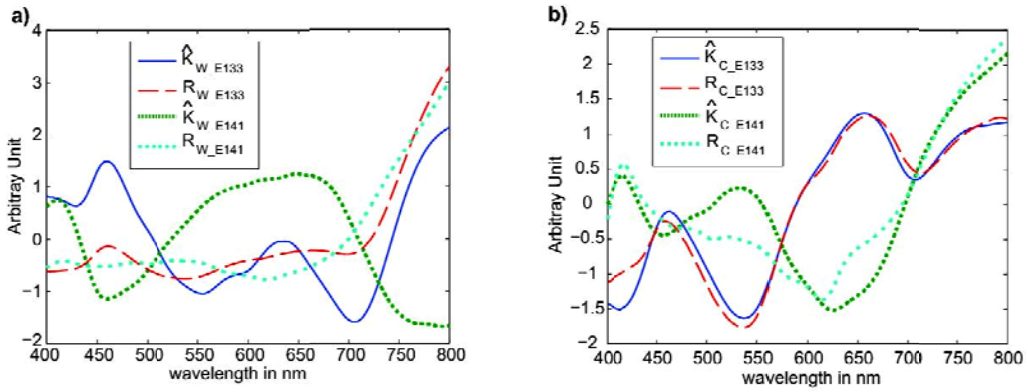

Figure 4 : Comparison of the raw and the corrected spectra acquired on the two coloring powders ($R_{w\_E133}(\lambda)$, $R_{w\_E141}(\lambda)$ and $R_{c\_E133}(\lambda)$, $R_{c\_E141}(\lambda)$) with the demixed pure spectrum ($K_{w\_E133}(\lambda)$, $K_{w\_E141}(\lambda)$ and $K_{c\_E133}(\lambda)$, $K_{c\_E141}(\lambda)$) extracted respectively from ($\mathbf{R_w}$) and ($\mathbf{R_c}$) with Linear unmixing.

Table 1: Figure of merit of the calibration models

	Cal set (n)	Test set (n)	Spectra	Predicted absorber	PLS factors	R^2	SEPc (% $g.L^{-1}$)
General model	S_1+S_2 (42)	S_1 (12)	$\mathbf{R_w}$	E133 E141	8 5	0.75 0.91	2.52 1.3
			$\mathbf{R_c}$	E133 E141	5 4	0.91 0.93	1.41 1.12

Table 2: Figure of merit of the calibration model built with samples of one particle size (S_2) and tested on samples with another particle size (S_1)

	Cal set (n)	Test set (n)	Spectra	Predicted absorber	PLS factors	R^2	SEPc (% $g.L^{-1}$)
General model	S_2 (21)	S_1 (12)	$\mathbf{R_w}$	E133 E141	5 5	0.69 0.83	3.33 1.79
			$\mathbf{R_c}$	E133 E141	4 3	0.91 0.93	1.72 1.73